[DOI]10.12016/j.issn.2096-1456.202550372

·生物材料专栏 基础研究·

镁锶共掺杂羟基磷灰石矿化胶原的构建与体外促成骨活性研究

王萌[1]，孙艺菲[2]，曹晓庆[3]，魏一源[4]，陈蕾[4]，张正龙[4]，慕昭[2]，朱娟芳[1]，牛丽娜[2]
1.郑州大学第一附属医院口腔医学中心，郑州大学口腔医学院，河南 郑州(450052)；2.口颌系统重建与再生全国重点实验室，国家口腔疾病临床医学研究中心，陕西省口腔医学重点实验室，空军军医大学口腔医院修复科，陕西 西安(710032)；3.新乡医学院第三附属医院口腔修复科，河南 新乡(453000)；4.兰州大学口腔医学院，甘肃 兰州(730000)

【摘要】 目的 探讨镁锶共掺杂羟基磷灰石矿化胶原(magnesium-strontium co-doped hydroxyapatite mineralized collagen，MSHA/Col)在改善骨修复微环境、提升骨再生能力方面的效果，为解决传统羟基磷灰石矿化胶原(hydroxyapatite mineralized collagen，HA/Col)支架组分仿生度不足与生物活性有限的问题提供思路。**方法** 制备高分子量聚丙烯酸稳定的镁锶共掺杂无定形磷酸钙前驱体(high-molecular-weight polyacrylic acid-stabilized amorphous calcium magnesium strontium phosphate precursor，HPAA/ACMSP)，通过高分辨率透射电子显微镜和能谱仪表征HPAA/ACMSP形貌及元素分布。将重组胶原海绵块于HPAA/ACMSP矿化液中浸泡，诱导镁锶共掺杂羟基磷灰石在胶原纤维内沉积(实验组：MSHA/Col；对照组：HA/Col)，扫描电子显微镜观察MSHA/Col形貌特征，通过X射线衍射和傅里叶红外光谱解析其晶体结构与化学组成，通过热重分析评估其矿物相占比，并测定支架的孔隙率、离子释放及体外降解性能。细胞学实验采用CCK-8法、活/死细胞染色、碱性磷酸酶染色、茜素红染色、RT-qPCR及蛋白质免疫印迹法，分别评估MSHA/Col支架对小鼠胚胎成骨细胞前体细胞系(MC3T3-E1)细胞增殖、存活、成骨分化早期活性、晚期矿化能力以及关键成骨标志物[Runt相关转录因子2(runt-related transcription factor 2，Runx2)、Ⅰ型胶原(collagen typeⅠ，Col-Ⅰ)、骨桥蛋白(osteopontin，Opn)、骨钙素(osteocalcin，Ocn)]基因和蛋白表达水平的影响。**结果** HPAA/ACMSP在透射电镜下呈非晶态球形纳米颗粒，能谱分析显示碳、氧、钙、磷、镁、锶元素均匀分布。MSHA/Col的扫描电子显微镜结果表明成功实现完全纤维内矿化，元素分析结果表明镁的质量分数为0.72%，与天然骨内镁含量匹配，锶的质量分数为2.89%；X射线衍射显示存在羟基磷灰石晶体特征峰(25.86°、31°~34°)；红外光谱结果显示，材料出现胶原及羟基磷灰石特征吸收峰；热重分析结果表明，材料中矿物相占比为78.29%，支架孔隙率为91.6%±1.1%，接近天然骨组织水平；离子释放曲线显示，Mg^{2+}、Sr^{2+}均表现出持续的释放行为；体外降解速率与新生骨组织的长入速率相匹配。细胞学实验表明，MSHA/Col显著促进MC3T3-E1细胞增殖(72 h活性提升130%，$P<0.001$)，具有优异的促成骨分化效能，能显著上调成骨相关基因及蛋白(Runx2、Col-Ⅰ、Opn、Ocn)的表达($P<0.01$)。**结论** MSHA/Col支架通过组分-结构双重仿生天然骨，在基因和蛋白水平上有效促进成骨分化，突破单纯羟基磷灰石矿化胶原的功能局限，为功能性骨修复材料开发提供新策略。

【关键词】 仿生矿化胶原；镁锶共掺杂；无定形磷酸钙；羟基磷灰石；纤维内矿化；骨再生；成骨分化；骨修复支架
【中图分类号】 R78 **【文献标志码】** A **【文章编号】** 2096-1456(2026)01-0015-14
【引用著录格式】 王萌，孙艺菲，曹晓庆，等. 镁锶共掺杂羟基磷灰石矿化胶原的构建与体外促成骨活性研究[J]. 口腔疾病防治, 2026, 34(1): 15-28. doi:10.12016/j.issn.2096-1456.202550372.

微信公众号

【收稿日期】 2025-08-26；**【修回日期】** 2025-10-27
【基金项目】 国家自然科学基金项目(22205257；82301043)
【作者简介】 王萌，硕士研究生在读，Email：wmeng0909@163.com
【通信作者】 牛丽娜，教授，博士，Email：niulina831013@126.com；朱娟芳，教授，博士，Email：zhujuanf72@163.com；慕昭，教授，博士，Email：zhaomu1994@126.com

Construction and *in vitro* osteogenic activity study of magnesium-strontium co-doped hydroxyapatite mineralized collagen

WANG Meng[1], SUN Yifei[2], CAO Xiaoqing[3], WEI Yiyuan[4], CHEN Lei[4], ZHANG Zhenglong[4], MU Zhao[2], ZHU Juanfang[1], NIU Lina[2]　1. Department of Stomatology, The First Affiliated Hospital of Zhengzhou University, School of Stomatology, Zhengzhou University, Zhengzhou 450052, China.　2. State Key Laboratory of Oral & Maxillofacial Reconstruction and Regeneration, National Clinical Research Center for Oral Diseases, Shaanxi Key Laboratory of Stomatology, Department of Prosthodontics, School of Stomatology, Air Force Medical University, Xi'an 710032, China.　3. Department of Prosthodontics, The Third Affiliated Hospital of Xinxiang Medical University, Xinxiang 453000, China.　4. School of Stomatology, Lanzhou University, Lanzhou 730000, China
Corresponding author: NIU Lina, Email: niulina831013@126.com; ZHU Juanfang, Email: zhujuanf72@163.com; MU Zhao, Email: zhaomu1994@126.com

【Abstract】 Objective　To investigate the efficacy of magnesium-strontium co-doped hydroxyapatite mineralized collagen (MSHA/Col) in improving the bone repair microenvironment and enhancing bone regeneration capacity, providing a strategy to address the insufficient biomimetic composition and limited bioactivity of traditional hydroxyapatite mineralized collagen (HA/Col) scaffolds. **Methods**　A high-molecular-weight polyacrylic acid-stabilized amorphous calcium magnesium strontium phosphate precursor (HPAA/ACMSP) was prepared. Its morphology and elemental distribution were characterized by high-resolution transmission electron microscopy (TEM) and energy-dispersive spectroscopy. Recombinant collagen sponge blocks were immersed in the HPAA/ACMSP mineralization solution. Magnesium-strontium co-doped hydroxyapatite was induced to deposit within collagen fibers (experimental group: MSHA/Col; control group: HA/Col). The morphological characteristics of MSHA/Col were observed using scanning electron microscopy (SEM). Its crystal structure and chemical composition were analyzed by X-ray diffraction and Fourier transform infrared spectroscopy, respectively. The mineral phase content was evaluated by thermogravimetric analysis. The scaffold's porosity, ion release, and in vitro degradation performance were also determined. For cytological experiments, CCK-8 assay, live/dead cell staining, alkaline phosphatase staining, alizarin red S staining, RT-qPCR, and western blotting were used to evaluate the effects of the MSHA/Col scaffold on the proliferation, viability, early osteogenic differentiation activity, late mineralization capacity, and gene and protein expression levels of key osteogenic markers [runt-related transcription factor 2 (Runx2), collagen type Ⅰ (Col-Ⅰ), osteopontin (Opn), and osteocalcin (Ocn)] in mouse embryonic osteoblast precursor cells (MC3T3-E1). **Results**　HPAA/ACMSP appeared as amorphous spherical nanoparticles under TEM, with energy spectrum analysis showing uniform distribution of carbon, oxygen, calcium, phosphorus, magnesium, and strontium elements. SEM results of MSHA/Col indicated successful complete intrafibrillar mineralization. Elemental analysis showed the mass fractions of magnesium and strontium were 0.72% (matching the magnesium content in natural bone) and 2.89%, respectively. X-ray diffraction revealed characteristic peaks of hydroxyapatite crystals (25.86°, 31° - 34°). Infrared spectroscopy results showed characteristic absorption peaks for both collagen and hydroxyapatite. Thermogravimetric analysis indicated a mineral phase content of 78.29% in the material. The scaffold porosity was 91.6% ± 1.1%, close to the level of natural bone tissue. Ion release curves demonstrated sustained release behavior for both magnesium and strontium ions. The *in vitro* degradation rate matched the ingrowth rate of new bone tissue. Cytological experiments showed that MSHA/Col significantly promoted MC3T3-E1 cell proliferation (130% increase in activity at 72 h, $P < 0.001$). MSHA/Col exhibited excellent efficacy in promoting osteogenic differentiation, significantly upregulating the expression of osteogenesis-related genes and proteins (Runx2, Col-Ⅰ, Opn, Ocn) ($P < 0.01$). **Conclusion**　The MSHA/Col scaffold achieves dual biomimicry of natural bone in both composition and structure, and effectively promotes osteogenic differentiation at the genetic and protein levels, breaking through the functional limitations of pure hydroxyapatite mineralized collagen. This provides a new strategy for the development of functional bone repair materials.

【Key words】 biomimetic mineralized collagen; magnesium-strontium co-doping; amorphous calcium phosphate; hydroxyapatite; intrafibrillar mineralization; bone regeneration; osteogenic differentiation; bone repair scaffold
J Prev Treat Stomatol Dis, 2026, 34(1): 15-28.
【Competing interests】 The authors declare no competing interests.
This study was supported by the grants from National Natural Science Foundation of China (No. 22205257, No. 82301043).

骨缺损修复是骨科学、材料学、生物学及组织工程学等多学科交叉的重要前沿研究领域，备受学者关注。目前临床上用于修复骨缺损的材料主要有自体骨、异种骨、同种异体骨、脱钙骨基质、金属材料、生物陶瓷以及组织工程骨[1]等，然而现有的临床应用材料都存在许多不足[2]。由于自体骨材料存在供骨量不足的问题，而其他材料可能引发免疫排斥或生物活性不足[3]，因此促使了对新型人造骨生物材料的研发探索。传统人工骨材料成分和结构仿生度不足，难以实现与宿主骨的良好整合，因此开发具有高度仿生性的新型骨缺损修复材料已成为研究热点[4]。

理想的骨缺损修复材料应具备良好的生物安全性和骨诱导活性，并高度仿生天然骨的组织结构与成分，同时降解产物需能被机体代谢吸收或直接参与新骨形成。胶原作为骨骼的主要有机组分，长期应用于骨缺损修复材料领域[5]。既往的研究通过仿生矿化技术实现的纳米羟基磷灰石（hydroxyapatite，HA）沿Ⅰ型胶原纤维定向沉积[6]，在化学成分和微观结构上高度模拟天然骨基质[7]。然而，传统羟基磷灰石矿化胶原（hydroxyapatite mineralized collagen，HA/Col）支架仍存在一些缺陷，如缺乏主动调控骨代谢的生物学功能，对细胞成骨分化及血管生成的促进作用有限。天然骨组织存在由多种微量元素构成的动态微环境[8]，而传统HA/Col支架无法复现这种生理性离子环境及多元素协同调节机制，导致材料组分仿生度和成骨活性显著不足。镁（Magnesium，Mg）和锶（Strontium，Sr）作为骨组织关键微量元素，通过协同机制优化骨修复微环境。镁可通过调节相关激素及因子影响骨代谢[9]，比如Mg^{2+}可通过下调促炎细胞因子抑制破骨细胞生成，并调节骨组织微环境以募集成骨细胞参与骨再生[10]，同时激活整合素-FAK-ERK级联反应，促进细胞增殖[11]。锶作为一种具有骨靶向特性的微量元素[12-13]，可通过增强碱性磷酸酶表达与活性，驱动间充质干细胞向成骨谱系定向分化，加速骨基质沉积与矿化进程[14]。

本研究创新性提出双离子协同作用策略：通过构建镁锶共掺杂羟基磷灰石矿化胶原（magnesium-strontium co-doped hydroxyapatite mineralized collagen，MSHA/Col），实现仿生组分重构和功能耦合，使支架中镁的质量分数为0.72%，精确匹配天然骨基质，锶质量分数为2.89%，通过锶促新骨形成与镁抑制破骨、促细胞增殖的协同机制，突破传统HA/Col的功能瓶颈，为提高传统HA/Col支架骨缺损修复材料仿生度提供了一种新的制备策略。

1　材料和方法

1.1　主要试剂和仪器

重组Ⅰ型胶原海绵（Ace Surgical Supply Co.，Inc，美国），聚丙烯酸（181285，Sigma-Aldrich，美国），无水氯化钙（C805228，麦克林，中国），磷酸氢二钾（P112220，阿拉丁，中国），无水氯化镁（M113689，阿拉丁，中国），无水氯化锶（S823438，麦克林，中国），MEM完全培养基（PM150411B，普诺赛，中国），胰蛋白酶（PB180229，普诺赛，中国），CCK-8试剂盒（C0038，碧云天，中国），碱性磷酸酶定量及染色试剂盒（C3206，碧云天，中国），茜素红染色液（ALIR-10001，赛业，中国），柱式法RNA提取试剂盒（9767，Takara，日本），Premix型反转录试剂（RR036A，Takara，日本），定量PCR试剂盒（RR420A，Takara，日本），一抗：Runx2兔多克隆抗体（20700-1-AP，Proteintech，美国，使用稀释比例1∶500），Opn兔多克隆抗体（22952-1-AP，Proteintech，美国，使用稀释比例1∶1 000），Ocn兔多克隆抗体（16157-1-AP，Proteintech，美国，使用稀释比例1∶1 000），Col-Ⅰ兔单克隆抗体（83752-3-RR，Proteintech，美国，使用稀释比例1∶1 000），二抗：HRP标记山羊抗兔IgG（Sa00001-2，Proteintech，美国，使用稀释比例1∶5 000）。

精密电子分析天平（EX223，OHAUS，美国），赛洛捷克磁力搅拌器（MS-H-Pro，SCILOGEX，美国），场发射扫描电子显微镜（SU9000II，Hitachi，日本），高分辨率透射电子显微镜（2100F，JEOL，日本），冷冻干燥机（LyoQuest，Teslstar，西班牙），热重分析仪（SDT650，TA Instruments，美国），酶标仪（Multiskan，Thermo，美国），荧光定量PCR仪器（CFX Connect，BIO-RAD，美国），电泳仪（1658033，BIO-RAD，美国），转膜仪（1704150，BIO-RAD，美国），化学发光成像系统（C300，Azure，美国）。

1.2　高分子量聚丙烯酸稳定的镁锶共掺杂无定形磷酸钙前驱体（high-molecular-weight polyacrylic acid-stabilized amorphous calcium magnesium strontium phosphate precursor，HPAA/ACMSP）的构建

A液：Tris缓冲液（0.96 g三羟甲基氨基甲烷、8.77 g氯化钠、6.61 g Tris-HCl溶于去离子水，定容至1 L，pH=7.30）中加入无水氯化钙、无水氯化锶

及高分子量聚丙烯酸(high molecular weight polyacrylic acid, HPAA),磁力混匀后使Ca^{2+}、Sr^{2+}、HPAA的浓度分别为9 mmol/L、0.9 mmol/L、0.1 mg/mL。加入无水氯化镁,使Mg^{2+}浓度为1.8、0.9、0.6 mmol/L。B液:4.2 mmol/L的磷酸氢二钾溶液。混合A、B液,磁力混匀,得到HPAA稳定的镁锶共掺杂无定形磷酸钙前驱体矿化液。

研究表明,低剂量锶具有良好促成骨、抑制破骨的能力[15]。而高剂量锶可能引发毒性[16],并且掺杂摩尔比(Sr^{2+}:Ca^{2+})高于15%时会显著影响羟基磷灰石的结晶度[17]。鉴于此,本研究采用Sr^{2+}:Ca^{2+}摩尔比为1∶10的锶掺杂浓度。Mg^{2+}通过协调骨代谢相关激素表达、下调促炎因子抑制破骨细胞生成,并可促进细胞增殖。然而Mg^{2+}可抑制ACP向HA的相变[18],为平衡Mg^{2+}掺杂与ACP相变过程,在矿化液中添加不同浓度的Mg^{2+}(使Mg^{2+}:Ca^{2+}摩尔比为1∶5、1∶10、1∶15),制备出不同含镁量的HPAA/ACMSP纳米复合物。HPAA稳定的无定形磷酸钙前驱体(high-molecular-weight polyacrylic acid-stabilized amorphous calcium phosphate precursor, HPAA/ACP)的配制不含氯化锶和氯化镁,其余步骤同上。

1.3　HPAA/ACMSP的透射电镜观察

利用高分辨率透射电子显微镜(high-resolution transmission electron microscopy, HRTEM)观测HPAA/ACMSP纳米复合体形态特性及粒径。使用能谱仪(energy dispersive X-ray spectroscopy, EDX)分析元素分布。

1.4　镁锶共掺杂羟基磷灰石矿化胶原(magnesium-strontium co-doped hydroxyapatite mineralized collagen, MSHA/Col)的制备

将2 cm × 2 cm × 0.2 cm的重组胶原海绵块经去离子水3次漂洗后,于HPAA/ACMSP矿化液中浸泡7 d,每日更新矿化液。矿化完成后依次用无水乙醇和去离子水各冲洗3次,-80 ℃冷冻24 h,随后置于冷冻干燥机中进行真空干燥。将得到的MSHA/Col真空储存或用于后续检测。使用HPAA/ACP矿化液制备羟基磷灰石矿化胶原(hydroxyapatite mineralized collagen, HA/Col)作为对照组[19]。

1.5　MSHA/Col形貌观察及理化性能分析

材料喷金后,使用扫描电子显微镜(scanning electron microscope, SEM)观察MSHA/Col表面特征,使用傅里叶红外光谱(fourier transform infrared spectroscopy, FTIR)和X射线衍射(X-ray diffraction, XRD)评价MSHA/Col的化学键构成及物相特性,并使用热重分析(thermogravimetric analysis, TGA)检测材料矿物质含量。

1.6　MSHA/Col孔结构、离子释放及体外降解性能测定

通过液体位移法测定Col、HA/Col、MSHA/Col支架的孔隙率。在量筒中加入8 mL无水乙醇,随机选取1个圆柱状支架在无水乙醇中浸没,使用封口膜将量筒口封闭,避免乙醇蒸发造成的误差。静置5 min后,记录无水乙醇体积并记录体积,然后将支架取出,再次记录剩余乙醇的体积,每种支架测定5个圆柱状支架并计算平均孔隙率。为了研究离子释放曲线,将MSHA/Col(5 mg)浸泡在10 mL PBS(pH 7.2, 0.01 mol/L)中,并在37 ℃下孵育14 d。在第1、3、7、14 d,离心后收集上清液,使用ICP-AES测定体外离子释放。进行了3次平行测量以求平均值。将质量为m_1的样品(Col、HA/Col、MSHA/Col)浸泡在含有胶原酶(0.01 g/mL)的磷酸盐缓冲液中,每2 d换液1次,将1、3、7、14 d的材料去除后冻干称量,质量记为m_2,每组3个平行样品,降解率(D)计算公式如下:$D=(m_1-m_2)/m_1\times 100\%$。

1.7　细胞培养与接种

采用小鼠胚胎成骨细胞前体细胞系(MC3T3-E1)作为实验细胞,采用含10% FBS和青链霉素双抗(100 U/mL)的α-MEM培养基,在37 ℃、5% CO_2孵箱中进行培养,每隔1 d更换培养液。当细胞密度达85%时,用胰蛋白酶消化细胞并进行传代。矿化胶原的消毒采用75%乙醇浸泡过夜,细胞接种前紫外照射至少2 h。

1.8　浸提液制备

将MSHA/Col与HA/Col分别置于15 mL离心管内,依照ISO10993标准:材料表面积和浸提液体积比值为1.25 cm^2/mL,加入完全培养基,37 ℃浸提72 h后,通过0.22 μm过滤器过滤制备各组材料浸提液,在无菌条件下完成封装,并于4 ℃冷藏保存以备使用。

1.9　细胞生物相容性测定

将MC3T3-E1细胞接种于96孔板,细胞密度为2×10^3个/孔,待细胞贴壁后弃原培养基,按实验分组设计(实验组:MSHA/Col;对照组:HA/Col;空白对照组:不做任何处理)加入制备的各组浸提液100 μL,在37 ℃、5% CO_2孵箱中进行培养,每24 h更换培养基。分别于接种后24、48及72 h采用

CCK-8法检测细胞增殖活性。接种后72 h，按照说明书使用活/死细胞染色试剂盒分别对活细胞和死细胞进行染色。

1.10　碱性磷酸酶及茜素红染色检测促成骨性能

将MC3T3-E1细胞接种于24孔板，细胞密度为1×10^5个/孔，每组设3个复孔，每孔加入1 mL细胞悬液。按照1.8中浸提液制备过程配制成骨诱导分化培养基的浸提液并保存备用。将24孔板置于培养箱中培养24 h，待细胞贴壁后，移除原培养基，按实验分组（同1.9）向每孔加入1 mL制备好的各组（MSHA/Col或HA/Col）成骨诱导分化培养基浸提液，空白对照组加入1 mL成骨诱导培养基。隔天换液。培养7 d后，谨慎吸除培养基，用PBS冲洗3次，随后按碱性磷酸酶试剂盒要求进行染色分析，使用体视显微镜拍摄图片。培养14 d后小心吸出培养基，用PBS冲洗3次，按照茜素红染色液说明书进行染色，使用体视显微镜拍摄图片。

1.11　RT-qPCR检测成骨分化相关基因表达

将MC3T3-E1细胞接种于6孔板，细胞密度为2×10^5个/孔，培养1 d后根据实验分组（同1.9）更换为2 mL成骨诱导分化培养基浸提液，每2 d换液1次。14 d后分别提取各孔总RNA并反转录为cDNA，利用RT-qPCR检测Runt相关转录因子2（runt-related transcription factor 2，Runx2）、Ⅰ型胶原（collagen type Ⅰ，Col-Ⅰ）、骨桥蛋白（osteopontin，Opn）、骨钙素（osteocalcin，Ocn）基因的mRNA表达水平。以β-肌动蛋白（β-actin）作为内参，使用比较Ct法（$2^{-\Delta\Delta Ct}$法）计算各组目的基因的相对表达水平。各基因的上下游引物见表1。

表1　RT-qPCR引物序列

Table 1　RT-qPCR Primer sequences

Gene	Primer sequence(5′→3′)
β-actin	F:AGATCAAGATCATTGCTCCTCC
	R:AAGGGTGTAAAACGCAGCTCA
Runx2	F:GACCTGCCACCTCTGCTT
	R:ATTGTGGGTTGGAGAGGG
Col-Ⅰ	F:GATGTTCACTTTGTGGACTC
	R:GGCCCTTAGCCATTGTTA
Opn	F:CCAGCCAAGGACCAACTACAA
	R:GTCGTCGTCATCATCGTCCA
Ocn	F:CCTCAACAATGGACTTGGAGCC
	R:GCTGTGCCGTCCATACTTTC

Runx2: runt-related transcription factor 2; Col-Ⅰ: collagen type Ⅰ; Opn: osteopontin; Ocn: osteocalcin

1.12　蛋白质免疫印迹法检测成骨分化相关蛋白表达

将MC3T3-E1细胞接种于6孔板，细胞密度为2×10^5个/孔，培养1 d后根据实验分组（同1.9）更换为2 mL成骨诱导分化培养基浸提液，每2 d换液1次。14 d后，弃去培养基，PBS清洗细胞，加入RIPA裂解液于冰上裂解提取总蛋白。通过BCA法测定蛋白浓度并定量。取等量蛋白样品进行十二烷基硫酸钠-聚丙烯酰胺凝胶电泳分离，随后转印至聚偏二氟乙烯膜。用5%脱脂牛奶封闭后，分别加入Runx2、Col-Ⅰ、Ocn、Opn及内参β-actin的一抗于4 ℃孵育过夜。TBST洗膜后，二抗室温孵育1 h，经增强化学发光试剂盒显影后，于成像系统下采集图像并分析目标蛋白的表达水平。

1.13　统计学分析

所有数据采用GraphPad Prism 8软件进行统计处理。当数据满足正态分布和方差齐性条件时，组间差异采用独立样本t检验进行比较，当数据不满足正态分布或方差不齐时，采用非参数的Kruskal-Wallis秩和检验进行组间比较。$P<0.05$为差异有统计学意义。

2　结　果

2.1　HPAA/ACMSP纳米复合物的制备与表征

制备出不同镁含量的HPAA/ACMSP纳米复合物，透射电镜结果显示，不同浓度Mg^{2+}组均形成了纳米级颗粒（图1）。能谱分析表明，不同浓度Mg^{2+}组的纳米颗粒中除了钙元素外，也存在镁、锶元素。红外测试表明，合成的无定形纳米复合物在910 cm^{-1}、1 036 cm^{-1}等处出现无定形磷酸钙中PO_4^{3-}的特征峰（图1）。表明所制备的纳米复合物呈无定形态，且离子掺杂并没有破坏无定形磷酸钙的结构特征。

进一步对HPAA/ACMSP进行高分辨透射电镜观察发现，HPAA/ACMSP纳米复合物呈现为球形颗粒。由于电子衍射图像的选定区域未出现显性的衍射环或斑点，可以证明HPAA/ACMSP为无定形状态；同时，元素能谱结果表明，来源于HPAA的碳、氧元素，与代表无定形磷酸钙镁锶的钙、磷、镁、锶元素分布一致，表明HPAA与无定形磷酸钙镁锶之间存在相互作用，形成了有机-无机的无定形纳米复合物（图2）。通过上述实验，证明成功合成了镁锶共掺杂无定形磷酸钙前驱体。

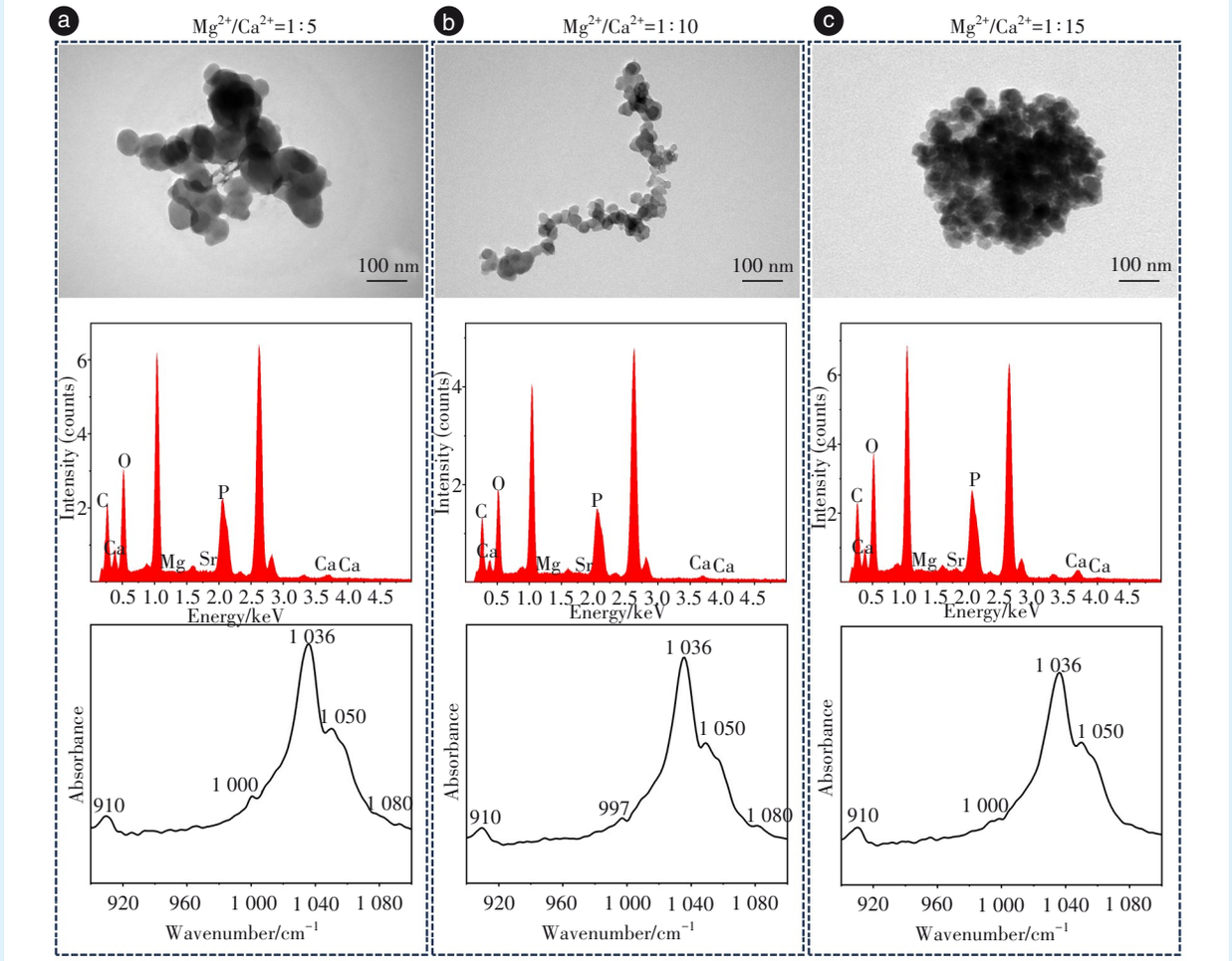

a: HPAA/ACMSP (high-molecular-weight polyacrylic acid-stabilized amorphous calcium magnesium strontium phosphate) nanocomposites (the Mg^{2+}/Ca^{2+} molar ratio equals 1∶5); b: HPAA/ACMSP nanocomposites (the Mg^{2+}/Ca^{2+} molar ratio equals 1∶10); c: HPAA/ACMSP nanocomposites (the Mg^{2+}/Ca^{2+} molar ratio equals 1∶15). TEM (transmission electron microscopy) analysis showed nanoparticle formation across all Mg^{2+} concentration groups and EDS (energy dispersive X-ray spectroscopy) confirmed the presence of Ca, Mg, Sr, P, C and O elements across all groups (the Sr^{2+}/Ca^{2+} molar ratio equals 1∶10), while characteristic PO_4^{3-} bands at 910 cm^{-1} and 1 036 cm^{-1} in FTIR (fourier transform infrared spectroscopy) spectra demonstrated preserved amorphous calcium phosphate (ACP) structure despite ion doping

Figure 1　Morphological and structural characterization of HPAA/ACMSP nanocomposites with varying Mg^{2+} concentrations

图1　不同Mg^{2+}浓度的HPAA/ACMSP纳米复合物的形貌及结构表征

2.2　不同Mg^{2+}浓度的HPAA/ACMSP矿化胶原效果

进一步使用不同镁含量的HPAA/ACMSP进行胶原纤维矿化相关实验，验证其诱导胶原纤维矿化的能力以及Mg^{2+}掺杂量对于胶原纤维内矿化的影响。结果显示，Mg^{2+}浓度显著影响胶原矿化程度。Mg^{2+}∶Ca^{2+}摩尔比1∶5时，矿化程度较低，胶原周期性结构清晰可见（图3a）；比例为1∶10时，矿化仍不充分，部分区域的胶原周期性结构仍可辨识（图3b）；当比例为1∶15时，胶原周期性条纹结构消失，表明其实现了完全的纤维内矿化（图3c）。综合上述结果，后续实验采用Sr^{2+}∶Ca^{2+}摩尔比1∶10与Mg^{2+}∶Ca^{2+}摩尔比1∶15的矿化液浓度制备HPAA/ACMSP，并用于胶原纤维矿化。

2.3　MSHA/Col与HA/Col的理化性能分析

如图4a~4f所示，由于矿物在胶原纤维内沉积，胶原的节律性条纹结构消失，通过能谱分析发现，MSHA/Col内Mg^{2+}质量分数为0.72%，与骨内镁含量接近，锶的质量分数为2.89%，而HA/Col组则未检测到Mg、Sr元素。X射线衍射分析证实两组材料的纤维中矿化相均为羟基磷灰石：在2θ=25.86°衍射角处出现的002衍射峰是羟基磷灰石晶体特征性的衍射峰，在31°~34°范围内观察到的特

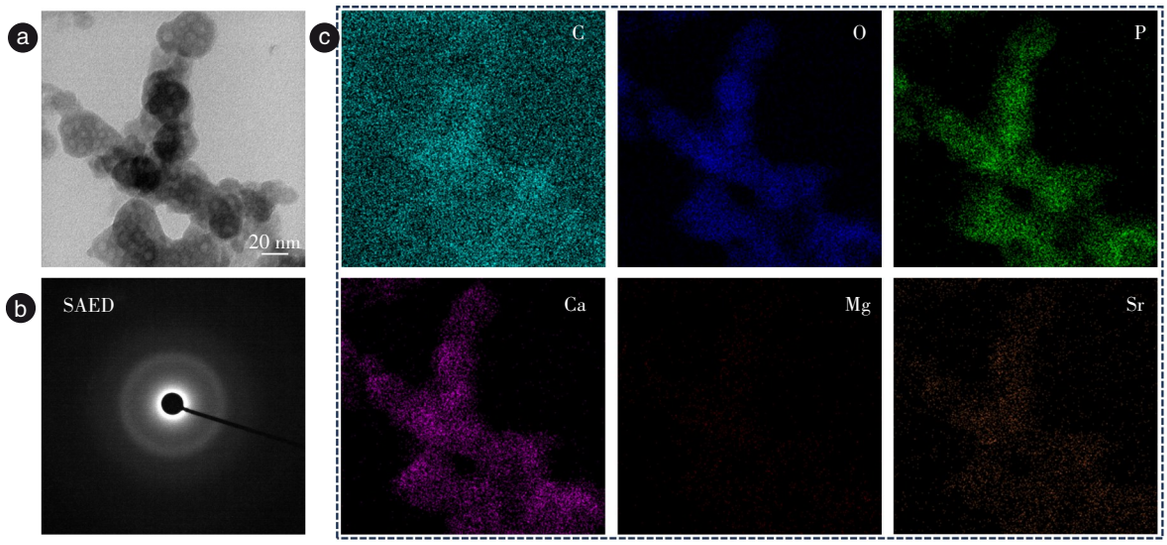

a: HRTEM (high-resolution transmission electron microscopy) confirmed spherical morphology of HPAA/ACMSP (high-molecular-weight polyacrylic acid-stabilized amorphous calcium magnesium strontium phosphate) nanoparticles with uniform size. b: SAED (selected area electron diffraction) patterns showed the amorphous structure due to absent diffraction rings and spots. c: EDS (energy dispersive X-ray spectroscopy) mapping illustrated homogeneous distribution of C, O, P, Ca, Mg, and Sr, indicating organic-inorganic interactions (the Sr^{2+}/Ca^{2+} molar ratio equals 1:10; the Mg^{2+}/Ca^{2+} molar ratio equals 1∶15)

Figure 2　High-resolution transmission electron microscopy images of HPAA/ACMSP nanocomposites and elemental analysis

图2　HPAA/ACMSP纳米复合物的高分辨率透射电镜图及元素分析

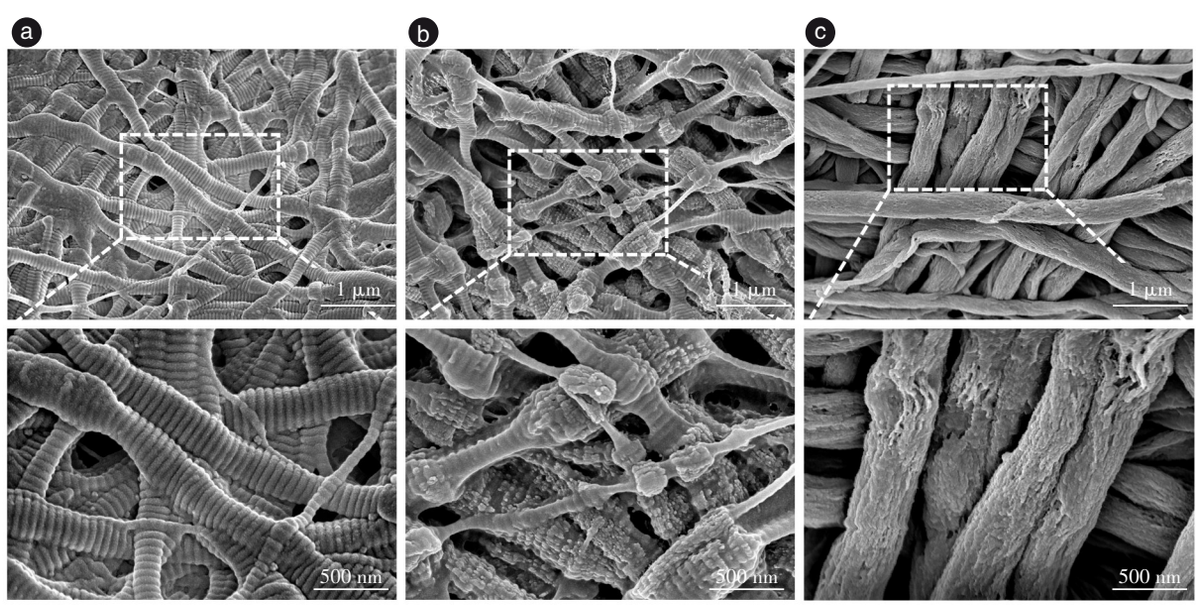

a: incomplete mineralization occurred with visible D-periodicity at Mg^{2+}/Ca^{2+} = 1∶5. b: partial mineralization appeared with residual periodic structure at Mg^{2+}/Ca^{2+} = 1∶10. c: complete intrafibrillar mineralization developed with obscured collagen bands at Mg^{2+}/Ca^{2+} = 1∶15 (the Sr^{2+}/Ca^{2+} molar ratio equals 1∶10). MSHA/Col: magnesium-strontium co-doped hydroxyapatite mineralized collagen

Figure 3　Scanning electron microscopy images of MSHA/Col under different Mg^{2+} concentrations

图3　不同Mg^{2+}浓度MSHA/Col扫描电镜图

征衍射峰与HA晶体的3个晶面(211,112和300)相对应(图4g)。MSHA/Col与HA/Col的红外光谱图(图4h)可见胶原特征峰(酰胺Ⅰ带在1 650 cm^{-1}处的C=O伸缩峰、酰胺Ⅱ带在1 550 cm^{-1}处NH弯曲峰),1 017 cm^{-1}处的特征峰对应磷酸根基团非对称伸缩振动(υ_3PO_4),而875和1 430 cm^{-1}处的吸收峰则归属于磷灰石晶体碳酸根基团的弯曲振动(υ_2CO_3和υ_3CO_3),表明矿化胶原的成功合成。热重分析(图4i)结果表明,仿生矿化7 d后MSHA/Col矿物含量达78.29%,而HA/Col组矿物含量为76.80%。两组材料的热降解行为均呈现阶段特征:59 ℃附近的吸热峰对应于结合水脱除,330~350 ℃区间的放热峰源于胶原蛋白分解,而持续的质量损失则反映了有机组分的逐步热解。

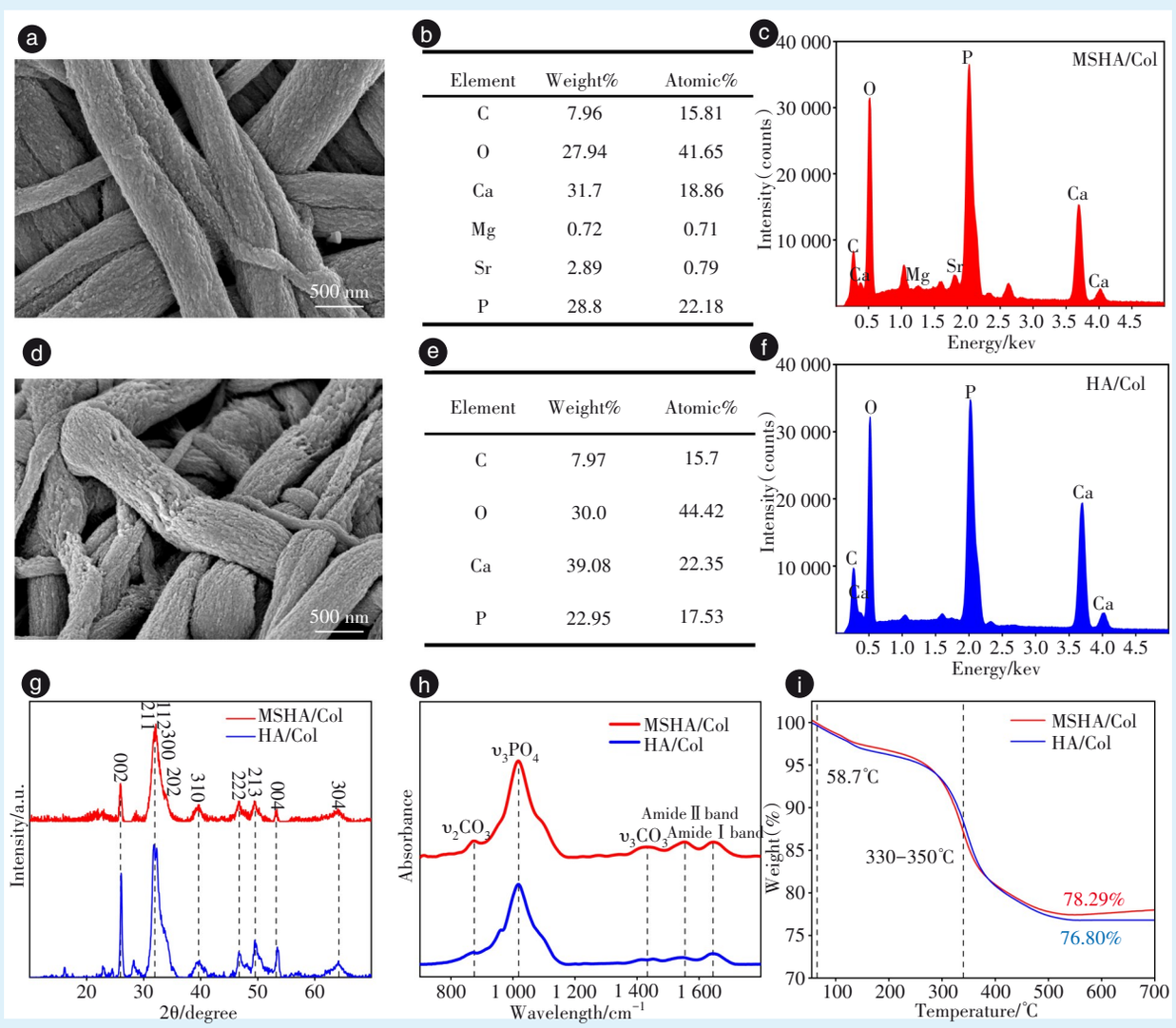

a: scanning electron microscopy (SEM) image of MSHA/Col (magnesium-strontium co-doped hydroxyapatite mineralized collagen) showing fully mineralized collagen fibers (Scale bar: 500 nm). b: energy-dispersive X-ray spectroscopy (EDS) quantitative analysis of MSHA/Col, indicating the presence of Mg (0.72 wt%) and Sr (2.89 wt%). c: elemental distribution maps of MSHA/Col. d: SEM image of HA/Col (hydroxyapatite mineralized collagen) showing fully mineralized collagen fibers (Scale bar: 500 nm). e: EDS quantitative analysis of HA/Col. f: elemental distribution maps of HA/Col. g: X-ray diffraction (XRD) patterns of MSHA/Col and HA/Col, showing characteristic hydroxyapatite peaks (e.g., 002 at 25.9° and 211/112/300 between 31° - 34°); h: fourier-transform infrared spectroscopy (FTIR) spectra of MSHA/Col and HA/Col, displaying collagen amide bands (Amide I at 1 650 cm^{-1}, Amide II at 1 550 cm^{-1}) and phosphate peaks (1 017 cm^{-1}, υ_3PO_4); i: thermogravimetric analysis (TGA) curves of MSHA/Col (mineral content: 78.29%) and HA/Col (mineral content: 76.80%)

Figure 4　Comparative morphological and physicochemical characterization of MSHA/Col and HA/Col

图4　MSHA/Col与HA/Col的形貌观察及理化性能对比分析

2.4　MSHA/Col支架的孔隙结构、离子释放及体外降解性能

为全面评估MSHA/Col支架作为骨修复材料的潜力，进一步对其多孔结构、离子释放行为及体外降解性能进行了表征。通过液体置换法计算，MSHA/Col支架呈现出相互连通的多孔网络结构，其孔隙率高达91.6% ± 1.1%（图5a），这一结构有利于细胞迁移、营养输送和血管长入。采用电感耦合等离子体发射光谱法对材料浸提液中的Mg^{2+}、Sr^{2+}浓度进行定时监测。离子释放曲线显示（图5b），Mg^{2+}、Sr^{2+}均表现出持续的释放行为，在前3 d内释放速率较快，随后进入一个缓慢而稳定的释放平台，直至14 d时仍能检测到有效的离子浓度。这种释放动力学特征有助于在骨修复早期及持续阶段为细胞提供必要的生物活性离子刺激。同时，通过体外浸泡实验评估了材料的降解性能。在2周的测试周期内，MSHA/Col支架的质量呈现缓慢下降的趋势，累计失重率为36.0% ± 1.5%（图5c），表明该材料具有良好的结构稳定性，其降解速率与新生骨组织的长入速率相匹配，避免了因过早崩解而导致的修复失败。

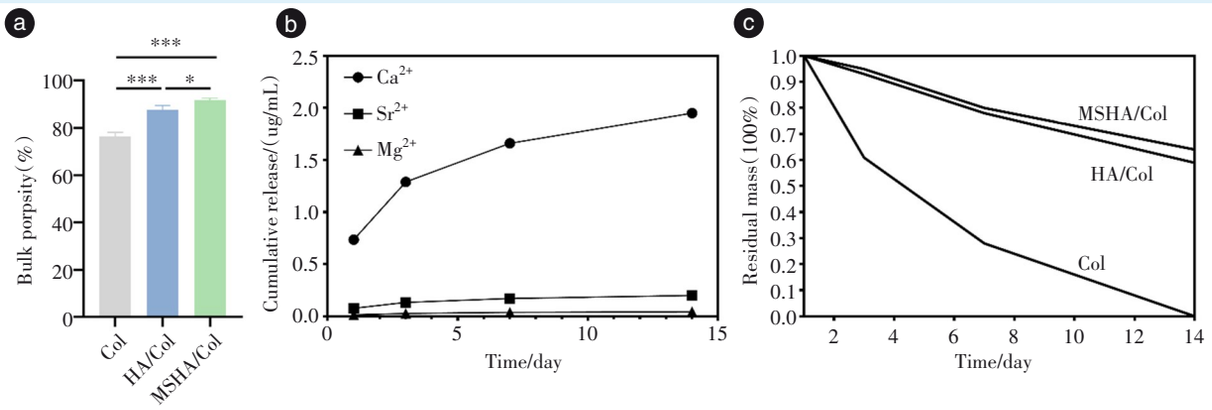

a: the porosity of the pure collagen (Col) scaffold, hydroxyapatite mineralized collagen (HA/Col) scaffold, and magnesium-strontium co-doped hydroxyapatite mineralized collagen (MSHA/Col) scaffold was measured by the liquid displacement method. The porosity of the MSHA/Col scaffold was measured to be 91.6% ± 1.1% by the liquid displacement method. Data are presented as mean ± SD (n = 3). *P < 0.05, ***P < 0.001. b: the cumulative release profiles of magnesium (Mg^{2+}) and strontium (Sr^{2+}) ions from the MSHA/Col scaffold in phosphate-buffered saline (PBS) over 1, 3, 7, and 14 days (n = 3) showed an initial rapid release phase within the first 3 days, followed by a sustained release plateau. c: the *in vitro* degradation profile of the MSHA/Col scaffold over 2 weeks, presented as cumulative mass loss (n = 3), demonstrated a slow degradation trend, with a final mass loss of 36.0% ± 1.5%, indicating good degradation stability

Figure 5　Porous structure, ion release, and *in vitro* degradation performance of MSHA/Col

图5　MSHA/Col支架的孔隙结构、离子释放及体外降解性能

2.5　细胞生物相容性测定

利用CCK-8对材料的生物相容性进行了测试，结果显示，在接种24、48、72 h后，MC3T3-E1细胞在MSHA/Col组中表现出持续的最高活性（图6a）。细胞活死染色分析表明，3组材料的细胞存活率未呈现显著差异（图6b）。这些实验结果证明，MSHA/Col具有良好的生物相容性。

2.6　促成骨性能测定

经7 d成骨诱导培养后，采用碱性磷酸酶染色法定量分析各组细胞的成骨分化潜能；继续培养至14 d时，通过茜素红染色法定性观察钙化结节的形成情况。实验结果表明，与对照组相比，MSHA/Col组不仅表现出最为显著的ALP染色阳性反应，同时在延长培养周期后还形成了大量致密、均匀分布的矿化结节，这一系列结果充分证实MSHA/Col具有优异的促成骨分化效能（图7）。

RT-qPCR结果显示，MSHA/Col组浸提液处理的细胞的Col-Ⅰ和Ocn表达均高于HA/Col组（图8），分别上调了约1.3倍、1.2倍（P<0.05），MSHA/Col组细胞的Runx2、Col-Ⅰ、Ocn和Opn表达均显著高于空白对照组，相对定量值分别上调了约1.6倍、4.4倍、1.9倍和3.0倍（P<0.01），从基因水平上表明MSHA/Col具有促进前成骨细胞向成骨细胞分化的能力。

为从蛋白质水平进一步验证MSHA/Col支架的

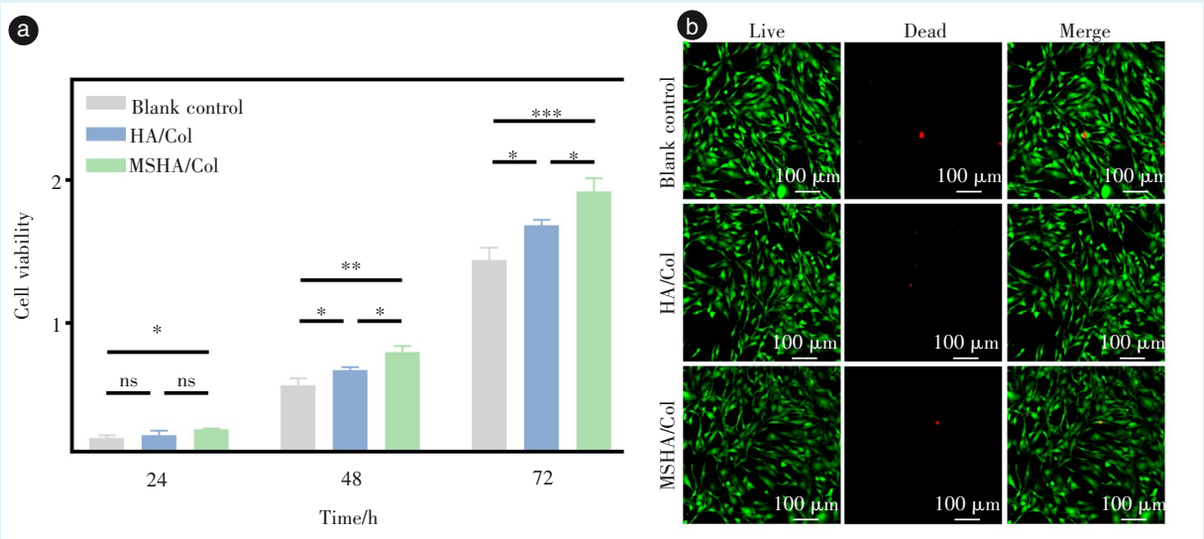

a: viability of MC3T3-E1 cells cultured in media containing extracts from blank control (culture medium without material extracts), hydroxyapatite mineralized collagen (HA/Col) scaffold, and magnesium-strontium co-doped hydroxyapatite mineralized collagen (MSHA/Col) scaffold for 24, 48, and 72 hours, as determined by CCK-8 assay. Data are presented as mean ± SD (n = 3). *P < 0.05, **P < 0.01, ***P < 0.001, ns: not significant. b: representative fluorescence images of live/dead staining after 72 hours of culture. Viable cells were stained green with calcein-AM, while dead cells were stained red with propidium iodide (PI). Scale bar: 100 μm

Figure 6　Cytocompatibility evaluation of MC3T3-E1 cells cultured with material extracts

图6　MC3T3-E1细胞经材料浸提液处理后的细胞生物相容性评价

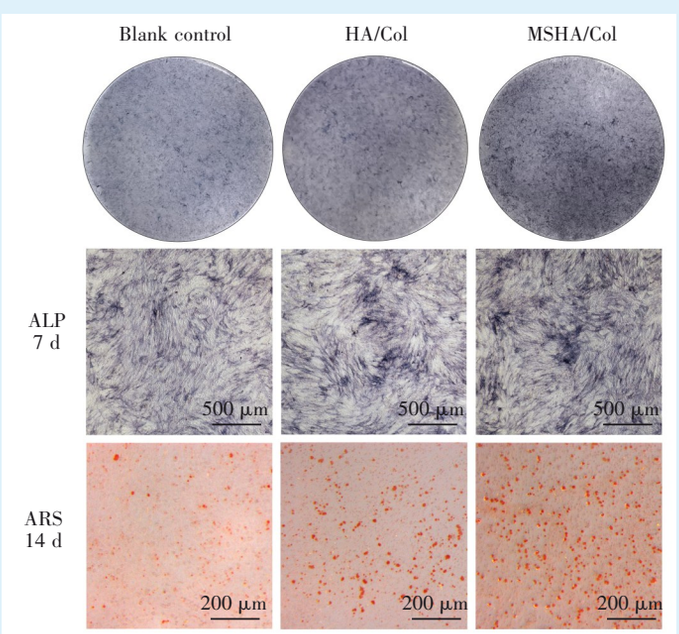

Representative images of alkaline phosphatase (ALP) staining (day 7) and alizarin red S (ARS) staining (day 14) of MC3T3-E1 cells following osteogenic induction culture with extracts from blank control (culture medium alone), HA/Col (hydroxyapatite mineralized collagen), and MSHA/Col (magnesium-strontium co-doped hydroxyapatite mineralized collagen)

Figure 7　Alkaline phosphatase and alizarin red S staining for evaluating osteogenic differentiation

图7　碱性磷酸酶及茜素红染色检测促成骨性能

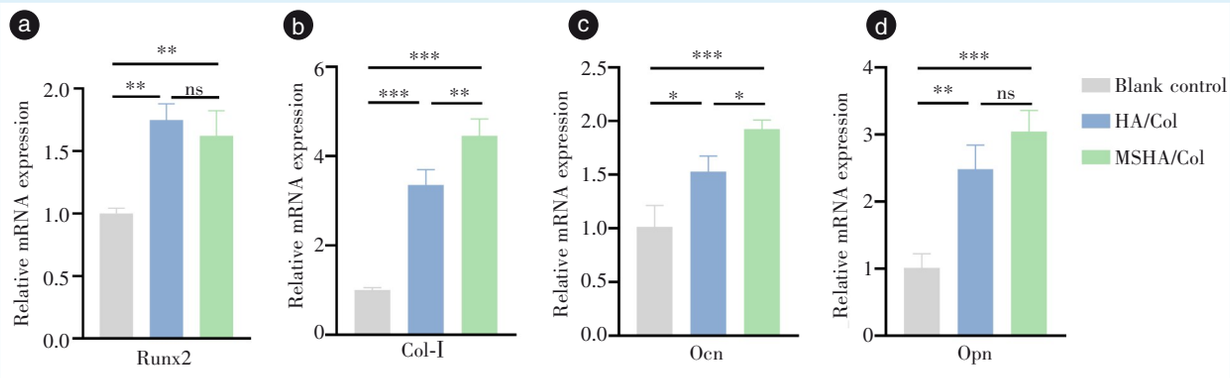

mRNA expression levels of osteogenesis-related genes in MC3T3-E1 cells cultured with extracts from blank control (culture medium without material extracts), hydroxyapatite mineralized collagen (HA/Col), and magnesium-strontium co-doped hydroxyapatite mineralized collagen (MSHA/Col) for 14 days. a: runt-related transcription factor 2 (Runx2); b: collagen type I (Col-I); c: osteocalcin (Ocn); d: osteopontin (Opn). *P < 0.05, **P < 0.01, ***P < 0.001, ns: not significant. Data are presented as mean ± SD (n = 3)

Figure 8　RT-qPCR was used to detect the effects of the MSHA/Col scaffold on the expression of osteogenesis-related genes in MC3T3-E1 cells

图8　RT-qPCR检测MSHA/Col支架对MC3T3-E1细胞成骨相关基因表达的影响

促成骨分化能力，通过蛋白质免疫印迹法检测了关键成骨标志物的表达。如图9a所示，与空白对照组和HA/Col组相比，MSHA/Col组中Runx2、Col-Ⅰ、Opn和Ocn的蛋白表达水平均呈现显著上调。对条带灰度值进行半定量统计分析的结果表明（图9b-9e），MSHA/Col组上述蛋白的相对表达量均显著高于空白对照组（P<0.05）。该结果与RT-qPCR检测到的基因表达上调趋势一致，从蛋白质翻译水平共同证实了MSHA/Col能有效促进MC3T3-E1细胞的成骨分化进程。

3　讨　论

本研究通过构建HPAA稳定的镁锶共掺杂无定形磷酸钙前驱体（HPAA/ACMSP），首次实现了镁锶双离子共掺杂矿化胶原支架（MSHA/Col）的原位合成。相较于传统羟基磷灰石修饰策略，镁锶共掺杂体系展现出显著的协同效应，ALP活性提升且成骨相关基因表达显著上调。支架中镁的质量分数精准控制在0.72%，匹配天然骨镁浓度，锶的质量分数为2.89%。这种组分仿生设计为细胞营造了类生理性微环境。在矿化动力学层面，HPAA/ACMSP的非晶态特性、HPAA的羧基螯合作用及Mg^{2+}作用协同延缓ACP相变，促使矿物深度渗透至胶原纤维间隙，最终形成高矿物占比的矿化结构[20-21]。

在骨缺损修复材料领域，无机离子因独特的生物学功能备受关注[22]。其中，锶具有促进骨形成的作用[23]，镁具有抑制破骨并促进细胞增殖的作用[24]。镁和锶常以多种形式应用，包括纯金属植入物、陶瓷涂层、可降解支架以及水凝胶微球缓释系统[25]等。镁合金因其可降解性和力学适配性曾被广泛研究，但存在腐蚀速率过快导致局部pH升高、氢气积聚等问题[26]；锶掺杂陶瓷虽能促进成骨，但脆性大、加工性能差，且高浓度锶可能导致异位钙化的发生[27]。这些材料往往存在离子释放不可控、与天然骨力学性能不匹配等缺陷。而传统羟基磷灰石矿化胶原（HA/Col）支架虽具生物相容性，却因缺乏活性离子协同调控机制[28]，无法复现天然骨的生理性成骨微环境，导致其组分仿生度与成骨活性显著不足。本研究通过仿生矿化技术使Mg^{2+}、Sr^{2+}以胶原纤维内矿化的形式沉积于纤维内部而并非表面修饰[29]，矿物相在胶原纤维内的纳米级分布可复现天然骨的有机-无机杂化结构[30]，实现活性离子在成骨过程中的缓释，既避免了金属植入物的腐蚀风险，又克服了陶瓷材料缺乏细胞外基质仿生的问题，改善传统HA/Col支架仿生度及成骨活性不足的缺陷，为骨再生提供持续刺激。从分子机制角度来看，Sr^{2+}可通过激活Wnt/β-catenin信号通路[31]，促进成骨相关转录因子Runx2的表达，进而上调Col-Ⅰ、Opn、Ocn等成骨标志基因的表达[32]，驱动间充质干细胞向成骨细胞分化及矿化结节形成。另一方面，Mg^{2+}不仅通过

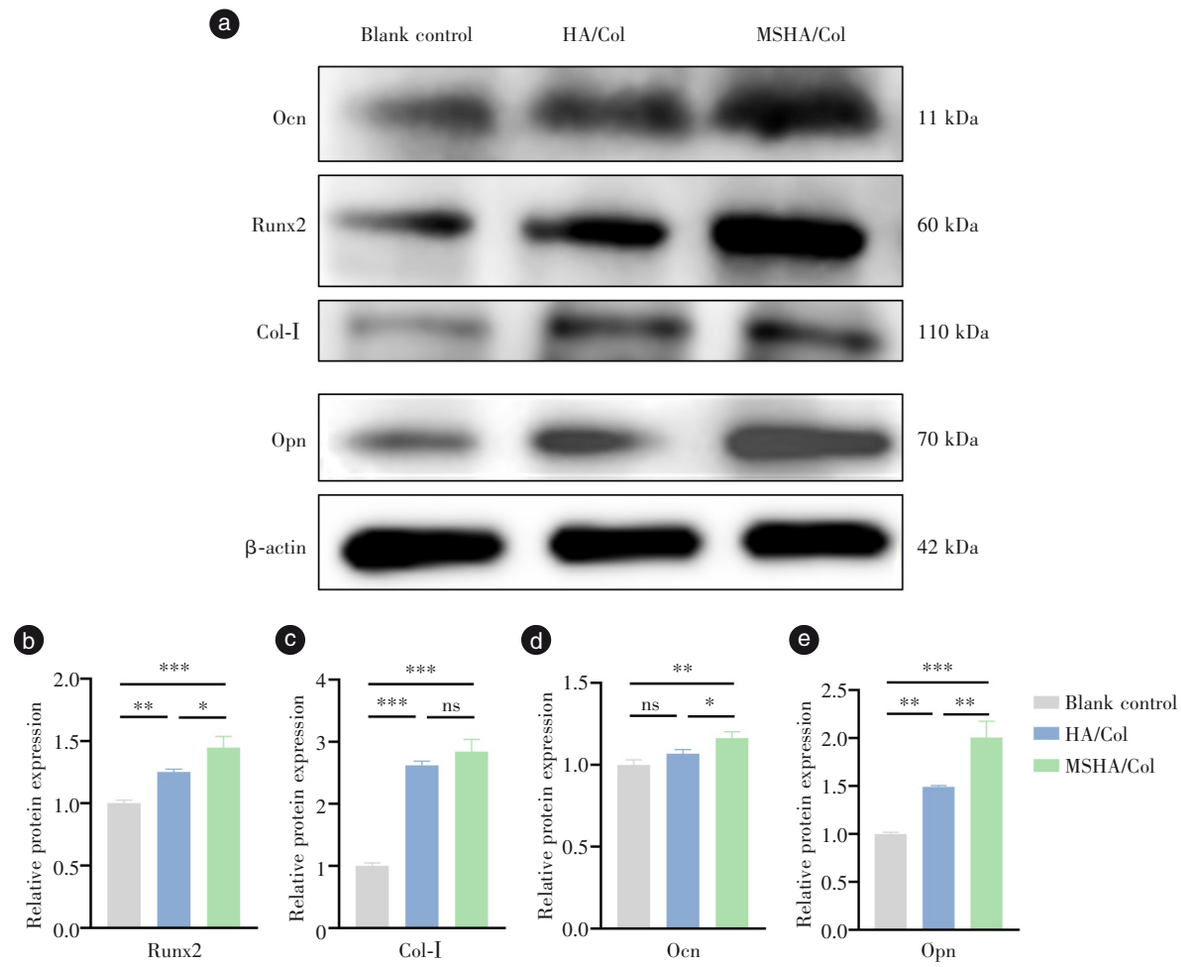

a: representative western blot images of runt-related transcription factor 2 (Runx2), collagen type I (Col-I), osteocalcin (Ocn), osteopontin (Opn), and the loading control β-actin in MC3T3-E1 cells after 14 days of osteogenic induction with extracts from blank control (culture medium without material extracts), hydroxyapatite mineralized collagen (HA/Col), and magnesium-strontium co-doped hydroxyapatite mineralized collagen (MSHA/Col). b – e: semi-quantitative analysis of the protein expression levels of Runx2(b), Col-Ⅰ (c), Ocn (d) , and Opn (e). *P < 0.05, **P < 0.01, *** P < 0.001, ns: not significant. Data are presented as mean ± SD (n = 3)

Figure 9　Western blotting was used to detect the effects of the MSHA/Col scaffold on the expression of osteogenesis-related proteins in MC3T3-E1 cells

图9　蛋白质免疫印迹法检测MSHA/Col支架对MC3T3-E1细胞成骨相关蛋白表达的影响

整合素-FAK-ERK通路促进细胞黏附与增殖[33]，还可能通过调节TRPM7离子通道影响细胞内镁稳态[34]，进而调控MAPK等信号通路，协同增强成骨细胞活性并抑制破骨细胞分化。此外，镁锶双离子可能通过交叉对话（crosstalk）机制，协同激活PI3K/AKT/GSK-3β通路，进一步稳定β-catenin，增强成骨基因的转录活性，形成正向调控环路[35]。因此，MSHA/Col支架通过多离子缓释与多通路协同，模拟天然骨微环境的动态调控网络，从而实现高效的骨再生促进效果。

然而，本研究仍存在一定局限性。首先，实验目前仅限于体外水平，未来需通过动物模型进一步验证材料在体内的骨整合能力、降解速率与骨再生的匹配性及长期生物安全性[35]。其次，Mg^{2+}、Sr^{2+}的比例调控虽为本体系的优势，但其最佳范围的确定仍需综合考虑微环境需求、释放动力学与细胞响应等多重因素[36]。过量镁会抑制矿化进程，而过量锶则可能引起细胞毒性，故未来应致力于建立离子比例与骨修复阶段的动态匹配关系，通过开发梯度或响应性释放系统，实现其在时空

维度上的精确调控，以推动个性化骨修复材料的发展。此外，作为一种仿生矿化构建的有机-无机复合材料，本支架的机械强度与天然皮质骨或金属陶瓷材料相比仍有差距，故更适用于非承重或低负荷区域的骨缺损修复，如颌骨囊肿术后腔性缺损、牙槽嵴增量及牙周骨缺损等。在这些场景中，材料的高孔隙率与优异的促成骨活性相较于绝对力学强度更具关键价值。未来工作将聚焦于通过交联策略或复合支架构建以提升其力学性能，从而拓展临床应用的潜力。

综上所述，本实验使用仿生矿化的方法在胶原纤维内引入镁锶离子共掺杂的羟基磷灰石，模拟天然骨生理性离子环境及多元素协同调节机制，为提高传统羟基磷灰石矿化胶原支架骨缺损修复材料仿生性和成骨活性提供一种新的制备策略。

【Author contributions】 Wang M performed the experiments and wrote the article. Sun YF, Cao XQ, Wei YY, Chen L, Zhang ZL performed the experiments, analyzed the data, revised the article. Mu Z, Zhu JF and Niu LN designed the study and reviewed the article. All authors read and approved the final manuscript as submitted.

参考文献

[1] Zhu G, Zhang T, Chen M, et al. Bone physiological microenvironment and healing mechanism: basis for future bone-tissue engineering scaffolds[J]. Bioact Mater, 2021, 6(11): 4110-4140. doi: 10.1016/j.bioactmat.2021.03.043.

[2] Li N, Wang J, Feng G, et al. Advances in biomaterials for oral-maxillofacial bone regeneration: spotlight on periodontal and alveolar bone strategies[J]. Regen Biomater, 2024, 11: rbae078. doi: 10.1093/rb/rbae078.

[3] Deng A, Zhang H, Hu Y, et al. Microsphere strategy to generate conformal bone organoid units with osteoimmunomodulation and sustainable oxygen supply for bone regeneration[J]. Adv Sci (Weinh), 2025, 12(32): e01437. doi: 10.1002/advs.202501437.

[4] Wu X, Yang H, Liu G, et al. Osteomimix: a multidimensional biomimetic cascade strategy for bone defect repair[J]. Adv Mater, 2025, 37(11): e2416715. doi: 10.1002/adma.202416715.

[5] Lesage C, Lafont M, Guihard P, et al. Material-assisted strategies for osteochondral defect repair[J]. Adv Sci (Weinh), 2022, 9(16): e2200050. doi: 10.1002/advs.202200050.

[6] Zhou Y, Hu Z, Jin W, et al. Intrafibrillar mineralization and immunomodulatory for synergetic enhancement of bone regeneration *via* calcium phosphate nanocluster scaffold[J]. Adv Healthc Mater, 2023, 12(12): e2201548. doi: 10.1002/adhm.202201548.

[7] Yang L, Kong J, Qiu Z, et al. Mineralized collagen-modified PMMA cement enhances bone integration and reduces fibrous encapsulation in the treatment of lumbar degenerative disc disease [J]. Regen Biomater, 2020, 7(2): 181-193. doi: 10.1093/rb/rbz044.

[8] Tong L, Liu Q, Xiong L, et al. Sustainably releasing osteogenic trace elements from montmorillonite intercalated hybrid nanocomposites accelerates bone regeneration[J]. Sci China Mater, 2024, 67 (7): 2067-2079. doi: 10.1007/s40843-023-2842-3.

[9] Zhu W, Wang W, Yang X, et al. Research progress on osteoclast regulation by biodegradable magnesium and its mechanism[J]. Regen Biomater, 2025, 12: rbaf026. doi: 10.1093/rb/rbaf026.

[10] Lin Z, Shen D, Zhou W, et al. Regulation of extracellular bioactive cations in bone tissue microenvironment induces favorable osteoimmune conditions to accelerate *in situ* bone regeneration[J]. Bioact Mater, 2021, 6(8): 2315-2330. doi: 10.1016/j. bioactmat.2021.01.018.

[11] Lötscher J, Martí I Líndez AA, Kirchhammer N, et al. Magnesium sensing *via* LFA-1 regulates $CD8^+$ T cell effector function[J]. Cell, 2022, 185(4): 585-602.e29. doi: 10.1016/j.cell.2021.12.039.

[12] Sun Y, Liu H, Sun XY, et al. *In vitro* and *in vivo* study on the osseointegration of magnesium and strontium ion with two different proportions of mineralized collagen and its mechanism[J]. J Biomater Appl, 2021, 36(3): 528-540. doi: 10.1177/0885328221101 6934.

[13] Geng Z, Li X, Ji L, et al. A novel snail-inspired bionic design of titanium with strontium-substituted hydroxyapatite coating for promoting osseointegration[J]. J Mater Sci Technol, 2021, 79: 35-45. doi: 10.1016/j.jmst.2020.11.041.

[14] Sekar Jeyakumar GF, Velswamy P, Gunasekaran D, et al. Enhancing the effectiveness of alkaline phosphatase and bone matrix proteins by tunable metal-organic composite for accelerated mineralization[J]. Int J Biol Macromol, 2023, 252: 126524. doi: 10.1016/j. ijbiomac.2023.126524.

[15] Liu X, Huang H, Zhang J, et al. Recent advance of strontium functionalized in biomaterials for bone regeneration[J]. Bioengineering (Basel), 2023, 10(4): 414. doi: 10.3390/bioengineering10040414.

[16] Sheng X, Li C, Wang Z, et al. Advanced applications of strontium-containing biomaterials in bone tissue engineering[J]. Mater Today Bio, 2023, 20: 100636. doi: 10.1016/j.mtbio.2023.100636.

[17] Li ZY, Lam WM, Yang C, et al. Chemical composition, crystal size and lattice structural changes after incorporation of strontium into biomimetic apatite[J]. Biomaterials, 2007, 28(7): 1452-1460. doi: 10.1016/j.biomaterials.2006.11.001.

[18] Ding H, Pan H, Xu X, et al. Toward a detailed understanding of magnesium ions on hydroxyapatite crystallization inhibition[J]. Cryst Growth Des, 2014, 14(2): 763-769. doi: 10.1021/cg401619s.

[19] Song Q, Jiao K, Tonggu L, et al. Contribution of biomimetic collagen-ligand interaction to intrafibrillar mineralization[J]. Sci Adv, 2019, 5(3): eaav9075. doi: 10.1126/sciadv.aav9075.

[20] Robin M, Mouloungui E, Castillo Dali G, et al. Mineralized collagen plywood contributes to bone autograft performance[J]. Nature, 2024, 636(8041): 100-107. doi: 10.1038/s41586-024-08208-z.

[21] Shan S, Tang Z, Sun K, et al. ACP-mediated phase transformation for collagen mineralization: a new understanding of the mechanism [J]. Adv Healthc Mater, 2024, 13(2): e2302418. doi: 10.1002/ adhm.202302418.

[22] Zhang L, Tang J, Han M, et al. Effect and mechanism of a

concentration-dependent inorganic ion biomimetic periosteum in a repairing bone defect[J]. Chem Eng J, 2023, 475: 146046. doi: 10.1016/j.cej.2023.146046.

[23] Zhou X, Wang Z, Li T, et al. Enhanced tissue infiltration and bone regeneration through spatiotemporal delivery of bioactive factors from polyelectrolytes modified biomimetic scaffold[J]. Mater Today Bio, 2023, 20: 100681. doi: 10.1016/j.mtbio.2023.100681.

[24] Zhao Z, Li G, Ruan H, et al. Capturing magnesium ions *via* microfluidic hydrogel microspheres for promoting cancellous bone regeneration[J]. ACS Nano, 2021, 15(8): 13041-13054. doi: 10.1021/acsnano.1c02147.

[25] Tao M, Cui Y, Sun S, et al. Versatile application of magnesium-related bone implants in the treatment of bone defects[J]. Mater Today Bio, 2025, 31: 101635. doi: 10.1016/j.mtbio.2025.101635.

[26] Ye J, Miao B, Xiong Y, et al. 3D printed porous magnesium metal scaffolds with bioactive coating for bone defect repair: enhancing angiogenesis and osteogenesis[J]. J Nanobiotechnology, 2025, 23(1): 160. doi: 10.1186/s12951-025-03222-3.

[27] Chen F, Tian L, Pu X, et al. Enhanced ectopic bone formation by strontium-substituted calcium phosphate ceramics through regulation of osteoclastogenesis and osteoblastogenesis[J]. Biomater Sci, 2022, 10(20): 5925-5937. doi: 10.1039/d2bm00348a.

[28] Radulescu DE, Vasile OR, Andronescu E, et al. Latest research of doped hydroxyapatite for bone tissue engineering[J]. Int J Mol Sci, 2023, 24(17): 13157. doi: 10.3390/ijms241713157.

[29] Li Z, Du T, Ruan C, et al. Bioinspired mineralized collagen scaffolds for bone tissue engineering[J]. Bioact Mater, 2020, 6(5): 1491-1511. doi: 10.1016/j.bioactmat.2020.11.004.

[30] Nanda R, Hazan S, Sauer K, et al. Molecular differences in collagen organization and in organic-inorganic interfacial structure of bones with and without osteocytes[J]. Acta Biomater, 2022, 144: 195-209. doi: 10.1016/j.actbio.2022.03.032.

[31] Wei B, Wang H, Niu J, et al. Strontium-doped layered double hydroxides with nitrate as interlayer anion reverse osteoporotic microenvironment *via* triple actions of pro-osteogenic, anti-osteoclastic and anti-inflammatory in osteoporosis therapy[J]. Chem Eng J, 2025, 523: 168567. doi: 10.1016/j.cej.2025.168567.

[32] 曹志炜, 杨雨青, 周陶, 等. 微量元素改性钛种植体表面研究进展[J]. 口腔疾病防治, 2020, 28(2): 107-111. doi: 10.12016/j.issn.2096-1456.2020.02.009.
Cao ZW, Yang YQ, Zhou T, et al. Research progress on trace elements-modified titanium implant surfaces[J]. J Prev Treat Stomatol Dis, 2020, 28(2): 107-111. doi: 10.12016/j.issn.2096-1456.2020.02.009.

[33] Yin D, Huang C, Liang C, et al. Magnesium regulates the migration and differentiation of NPMSCs *via* the integrin signaling pathway[J]. Curr Stem Cell Res Ther, 2025, 20(7): 768-783. doi: 10.2174/011574888X304570240705094512.

[34] Schmidt E, Narangoda C, Nörenberg W, et al. Structural mechanism of TRPM7 channel regulation by intracellular magnesium[J]. Cell Mol Life Sci, 2022, 79(5): 225. doi: 10.1007/s00018-022-04192-7.

[35] Ho CC, Hsu TT, Chiu YC, et al. 3D-printed magnesium/strontium-co-doped calcium silicate scaffolds promote angiogenesis and bone regeneration through synergistic bioactive ion stimulation[J]. J Biol Eng, 2025, 19(1): 58. doi: 10.1186/s13036-025-00528-6.

[36] Li C, Zhang W, Nie Y, et al. Time-sequential and multi-functional 3D printed MgO_2/PLGA scaffold developed as a novel biodegradable and bioactive bone substitute for challenging postsurgical osteosarcoma treatment[J]. Adv Mater, 2024, 36(34): e2308875. doi: 10.1002/adma.202308875.

（编辑　罗燕鸿）

官网